

Cost-Efficient Multi-Objective Design of Miniaturized Microwave Circuits Using Machine Learning and Artificial Neural Networks

Slawomir Koziel^{1,2}[0000-0002-9063-2647], Anna Pietrenko-Dabrowska²[0000-0003-2319-6782],
and Leifur Leifsson³[0000-0001-5134-870X]

- ¹ Engineering Optimization & Modeling Center, Department of Engineering, Reykjavik University, Menntavegur 1, 102 Reykjavik, Iceland
koziel@ru.is
- ² Faculty of Electronics Telecommunications and Informatics, Gdansk University of Technology, Narutowicza 11/12, 80-233 Gdansk, Poland
anna.dabrowska@pg.edu.pl
- ³ School of Aeronautics and Astronautics, Purdue University, West Lafayette, IN 47907, USA
leifur@purdue.edu

Abstract. Designing microwave components involves managing multiple objectives such as center frequencies, impedance matching, and size reduction for miniaturized structures. Traditional multi-objective optimization (MO) approaches heavily rely on computationally expensive population-based methods, especially when executed with full-wave electromagnetic (EM) analysis to guarantee reliability. This paper introduces a novel and cost-effective MO technique for microwave passive components utilizing a machine learning (ML) framework with artificial neural network (ANN) surrogates as the primary prediction tool. In this approach, multiple candidate solutions are extracted from the Pareto set via optimization using a multi-objective evolutionary algorithm (MOEA) applied to the current ANN model. These solutions expand the dataset of available (EM-simulated) parameter vectors and refine the surrogate model iteratively. To enhance computational efficiency, we employ variable-resolution EM models. Tested on two microstrip circuits, our methodology competes effectively against several surrogate-based approaches. The average computational cost of the algorithm is below three hundred EM analyses of the circuit, with the quality of generated Pareto sets surpassing those produced by the benchmark methods.

Keywords: Microwave design, multi-objective optimization, design automation, machine learning, neural networks, surrogate modeling, Pareto optimality.

1 Introduction

Contemporary microwave design confronts various challenges linked to meeting diverse performance criteria [1], [2], while concurrently striving for compact circuit sizes [3]-[5]. The miniaturization imperative is crucial for numerous applications like the Internet of

Things, mobile healthcare, and more [6]-[8]. Achieving size reduction involves strategies such as multi-layer implementations or integrating geometrical modifications like line meandering, compact microstrip resonant cells, metamaterials, etc. [9]-[11]. Accurate assessment of intricate circuits full-wave electromagnetic (EM) analysis is indispensable [20], which proves computationally demanding, especially when repetitive simulations are required (e.g., for optimization, uncertainty quantification [12], [13]). To mitigate these high computational costs, several techniques have been introduced, including space mapping [14], response correction [15], surrogate-assisted methods [16], response feature techniques [17], machine learning [18], or restricted Jacobian updating strategies [19].

Designing microwave systems involves managing multiple criteria simultaneously, encompassing aspects like center frequency, bandwidth, return loss levels, and more. Often, these design goals conflict with each other. For instance, in the case of miniaturization, reducing size might compromise electrical performance. Achieving the best possible design trade-offs often results in a Pareto set representation [20], necessitating multi-objective optimization (MO). Many available numerical optimization methods handle only scalar objectives, requiring objective aggregation for MO [21]. However, this approach yields a single design per algorithm run. Generating the entire Pareto set requires genuine MO [20], which is primarily conducted using bio-inspired population-based algorithms [22]-[26]. Clearly, nature-inspired methods can produce the entire set of trade-off designs in a single run, yet, they are computationally inefficient. Particularly, direct simulation-driven MO is constrained because of excessive CPU costs.

To address the high computational costs, surrogate modeling methods [27] offer an alternative by utilizing a rapid metamodel for system evaluation instead of resource-intensive EM analysis. Surrogates can either be pre-constructed [28], [29], or iteratively refined throughout the optimization run [30], [31]. However, building reliable surrogates over larger parameter spaces poses numerical challenges, making the former approach uncommon. Consequently, most multi-objective (MO) frameworks adopt a machine learning (ML) approach, refining the metamodel iteratively using EM data gathered during the search process. The surrogate model's role lies in generating candidate designs, known as infill points [32], with a wide array of ML techniques available in literature [33], [34]. Although cost-efficient, ML tends to leave a significant portion of the search space unexplored. The search process focuses on an initially identified promising region, allocating most resources to its exploration. Moreover, the challenges in building reliable data-driven models restrict ML's applicability to simpler problems.

Addressing the challenges of EM-driven multi-objective optimization (MO) associated with high parameter space dimensionality can be achieved through domain restriction. Practically, this is done by identifying extreme non-dominated solutions (requiring extra optimization runs for individual objectives) and delineating the domain using this data [35]. The computational benefits of domain restriction lie in the smaller training datasets needed within a reduced volume, enhancing the MO process's effectiveness. Another method, performance-driven modeling [36], constructs the surrogate only within the region housing high-quality designs. Similar to domain restriction, this approach significantly improves the surrogate's predictive capability while reducing the required training data samples [37]-[39]. However, the said algorithms might incur high initial costs due to acquiring extreme non-dominated solutions, which could easily reach hundreds of EM simulations. Additionally, there's an assumption about the regularity of the Pareto front, posing a limitation.

The aim of this article is to introduce an innovative approach for cost-effective and reliable multi-objective optimization (MO) of compact microwave circuits. The proposed algorithm leverages machine learning (ML) with artificial neural networks (ANN). An integral part of this algorithm is a multi-objective evolutionary algorithm (MOEA) used to optimize the ANN metamodel and generate a current representation of the Pareto set. From this set, a collection of candidate designs (infill points) is derived, and their EM-simulated circuit characteristics are acquired and integrated into the ongoing dataset. The termination criterion for the algorithm is based on evaluating the similarity between the rendered Pareto sets in successive iterations. To reduce CPU cost, variable-resolution EM simulations are employed. Initial sampling starts at the lowest acceptable fidelity, gradually increasing to higher levels later on. While lower-resolution EM analyses are faster, they lack accuracy. The search process's reliability is maintained by progressively removing low-resolution points from the dataset, retaining only high-fidelity ones to form the final Pareto set. The effectiveness of this approach has been validated using two miniaturized microwave circuits, demonstrating exceptional performance. The average running cost equates to fewer than three hundred high-fidelity EM analyses of the circuit under design. This represents almost ninety percent relative acceleration over one-shot benchmark algorithms and over forty percent speedup over single-fidelity ML frameworks. Importantly, the reported savings do not affect the quality of the resulting Pareto fronts.

This work encompasses several novel contributions, notably: (i) development and deployment of a high-efficiency machine learning framework tailored for the multi-criteria design of microwave circuits; (ii) integration of variable-resolution EM simulations into a model management strategy, facilitating accelerated optimization; (iii) successful demonstration of the proposed procedure's capability in managing complex multi-objective tasks, handling parameter space dimensions of up to fifteen.

2 Multi-Objective Optimization Methodology

This section explores the details of the developed MO algorithm, whose constituent parts include a machine learning (ML) framework, ANN models, and multi-resolution EM simulations. Sections 2.1 and 2.2 delineate the formulation of the MO problem and the variable-resolution EM models, respectively. The remaining sections are devoted to providing specifics of the introduced procedure, starting from sampling and ANN model construction (Section 2.3), through the usage of MOEA algorithm to generate the Pareto set (Section 2.4), infill point rendition (Section 2.5), and variable-fidelity model management (Section 2.6). Lastly, Sections 2.7 and 2.8 discuss the termination criteria, and reprise the entire MO framework, respectively.

2.1 MO Microwave Design Optimization

Our aim is to simultaneously minimize all considered objectives across the design space X . Hereinafter, the design objectives will be referred to as $F_k(\mathbf{x})$, $k = 1, \dots, N_{obj}$, whereas the vector of objectives will be referred to as $\mathbf{F}(\mathbf{x}) = [F_1(\mathbf{x}) \ F_2(\mathbf{x}) \ \dots \ F_{N_{obj}}(\mathbf{x})]^T$, with $\mathbf{x} = [x_1 \ \dots \ x_n]^T$ representing a designable vector (geometry parameters). The design space X is of interval-type and it is bound by lower and upper limits $\mathbf{l} = [l_1 \ \dots \ l_n]^T$, and $\mathbf{u} = [u_1 \ \dots \ u_n]^T$, respectively.

The objectives pertaining to real-world circuits are at least partially contradictory, as in the case of miniaturization which deteriorates electrical properties. When multiple objectives are present, Pareto dominance relation [40] is indispensable to compare various designs: given designs \mathbf{x} and \mathbf{y} , \mathbf{x} is said to dominate over \mathbf{y} , or $\mathbf{F}(\mathbf{y}) \prec \mathbf{F}(\mathbf{x})$ if and only if $F_k(\mathbf{y}) \leq F_k(\mathbf{x})$ for $k = 1, \dots, N_{obj}$, and $F_k(\mathbf{y}) < F_k(\mathbf{x})$ for not fewer than one k . Ultimately, MO aims at finding a set of globally non-dominated vectors within X , with \mathbf{x} being globally non-dominated if no $\mathbf{y} \in X$ such at $\mathbf{F}(\mathbf{y}) \prec \mathbf{F}(\mathbf{x})$ exists.

MO procedures heavily utilize nature-inspired algorithms: tremendously expensive when applied with microwave circuit simulation models, chiefly using full-wave EM analysis. To circumvent this issue, surrogate modeling techniques are used, oftentimes, within various ML frameworks. Yet, creating dependable surrogate models remains the primary challenge, especially in highly-dimensional parameter spaces with extensive parameter ranges. Our approach alleviates the mentioned issues to some point by combining ML, multiple infill point rendition, and variable-fidelity EM analysis.

2.2 Multi-Resolution EM Models

We employ computational models in the form of full-wave EM analysis. Usually, circuit design is carried out using a model ensuring adequate accuracy $\mathbf{R}_f(\mathbf{x})$, i.e., fine (or high-fidelity) model. Unfortunately, evaluation of $\mathbf{R}_f(\mathbf{x})$ tends to be expensive, with the cost increasing with structure complexity. Lower simulation times can be obtained for models of reduced fidelity, yet, accompanied with a simultaneous degradation of model reliability. Oftentimes, two levels of EM model resolution are utilized (high-/low-fidelity), yet, the prospective benefits of integrating a spectrum of resolutions have been recently shown [41].

This research exploits multi-resolution EM simulations to speed-up the multi-objective (MO) search process. In our approach, we utilize a continuous range of fidelities $L \in [L_{\min}, L_{\max}]$. Hereinafter, we will denote as $\mathbf{R}(\mathbf{x}, L)$ the EM model of fidelity L . Moreover, $\mathbf{R}_f(\mathbf{x}) = \mathbf{R}(\mathbf{x}, L_{\max})$ and $\mathbf{R}_c(\mathbf{x}) = \mathbf{R}(\mathbf{x}, L_{\min})$ will be used for high- and low-fidelity models, respectively.

2.3 Sampling Procedure and ANN-Based Surrogate Modeling

Our MO framework exploits surrogates in the form of ANN regression models. The premier metamodel is built utilizing data set comprising N_{init} samples $\mathbf{x}_B^{(j)}$, $j = 1, \dots, N_{\text{init}}$, collected over the design space X using an increased-efficacy Latin Hypercube Sampling (LHS) protocol [42]. At this step, EM simulations are carried out at the minimum level of fidelity L_{\min} , i.e., we have $\mathbf{R}(\mathbf{x}_B^{(j)}, L_{\min})$, $j = 1, \dots, N_{\text{init}}$.

As an ANN surrogate, we utilize a multi-layer perceptron [43] with the following setup: two hidden layers (each comprising 10 neurons), sigmoid activation function, network trained using Levenberg-Marquardt algorithm (maximum 1000 learning epochs, performance metric in the form of mean squared error, MSE, random split of testing/ training samples). In each iteration, the ANN model is trained anew. Using such a simple network allows for retaining short training duration (around dozen seconds for datasets comprising below two hundred samples). Thus, the cost of rendering ANNs is not taken into account in the total expenses of the MO algorithm. Figure 1 depicts the ANN-assisted rendition of frequency characteristics of a microwave coupler.

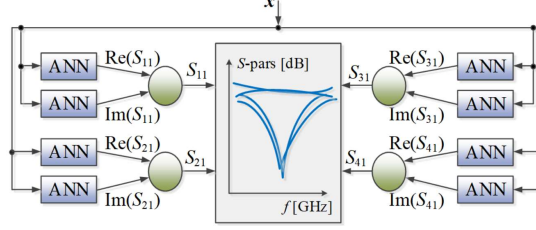


Fig. 1. Complex-valued scattering parameters of the microwave coupler represented using ANN model. ANN model renders outputs representing all pertinent device responses for specific frequencies f_1 through f_m .

Representation: Natural (floating point numbers);
Population replacement: Generational model (the new population supplants the former one); N_P stands for population size;
Selection: Pareto-ranking-based tournaments;
Other mechanisms:

- Fitness sharing with adaptively adjusted niche size;
- Multi-point elitism (non-dominated solution sets retained after each iteration);
- Termination condition based on a sufficient reduction of newly found Pareto-optimal solutions.

Recombination: A combination of an intermediate and arithmetic crossover (with equal probabilities $p_c/2$ each) [45]:

- Intermediate crossover: given $\mathbf{x} = [x_1 \dots x_n]^T$ and $\mathbf{y} = [y_1 \dots y_n]^T$ as the parent individuals, the offspring $\mathbf{z} = [z_1 \dots z_n]^T$ is obtained so that $z_i = \alpha x_i + (1-\alpha)y_i$ with $0 \leq \alpha \leq 1$ (α selected randomly);
- Arithmetic crossover: produces the offspring $\mathbf{z} = \alpha \mathbf{x} + (1-\alpha)\mathbf{y}$; $0 \leq \alpha \leq 1$ (α selected randomly);

Mutation: Localized random perturbations, applied with probability p_m , independently for each design variable. We have $x_i \rightarrow x'_i = x_i + \Delta x_i$, where Δx_i is a random deviation defined as [45]

$$\Delta x_i = \begin{cases} (x_{i,\max} - x_i) \cdot (2(r-0.5))^\beta & \text{if } r > 0.5 \\ (x_i - x_{i,\min}) \cdot (2(0.5-r))^\beta & \text{otherwise} \end{cases}$$

where $r \in [0,1]$ is a random number and $\beta = 3$

Fig. 2. The description of the search engine: multi-objective evolutionary algorithm (MOEA), which renders Pareto sets by carrying out ANN-surrogate-based multi-objective optimization.

2.4 Multi-Objective Evolutionary Algorithm (MOEA)

We employ multi-objective evolutionary algorithm (MOEA) as the main search mechanism which renders sets of Pareto-optimal designs by optimizing the ANN models. Our version of MOEA adheres to the principles included in [44]. Figure 2 illustrates the employed algorithm. The verification experiments of Section 3 utilize the following configuration of MOEA: $N_P = 200$ (population size), $p_{cross} = 0.1$ (crossover probability), and $p_{mut} = 0.8$ (mutation probability). The MOEA employs the rapid ANN model, rendering its CPU costs insignificant in comparison to that of an individual circuit EM simulation.

2.5 Infill Point Allocation

Each algorithm iteration involves generating N_{infill} candidate solutions, which are included into the set the algorithm operates on. The said infill vectors are derived from the latest Pareto front rendered by MOEA (see Section 2.4). Figure 3 depicts the selection procedure striving to accomplish a uniform coverage of the Pareto front (for a two-dimensional objective space). Towards this end, N_{infill} values of the objective F_2 are set as

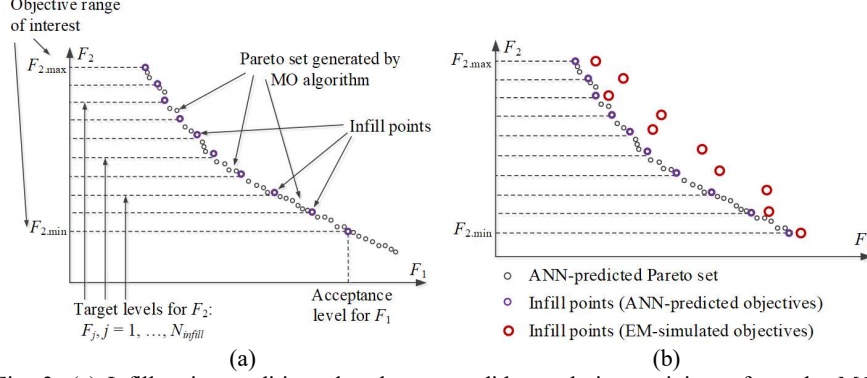


Fig. 3. (a) Infill point rendition: the chosen candidate solutions originate from the MOEA-generated Pareto front through ANN model optimization. We aim at an even distribution of the vectors concerning the objective F_2 , whose range is established by the span of the Pareto set (along with optional requirements, e.g., target value of the objective F_1 as depicted above); (b) Infill points: ANN-predicted vs. EM-evaluated. The EM-predicted objectives are inferior to the ANN-rendered ones due to low surrogate accuracy. The following situation is shown: if F_2 pertains to antenna footprint, values of F_2 are identical for EM-analysis and ANN render; still, EM-predicted levels of F_1 are inferior to that ANN-predicted.

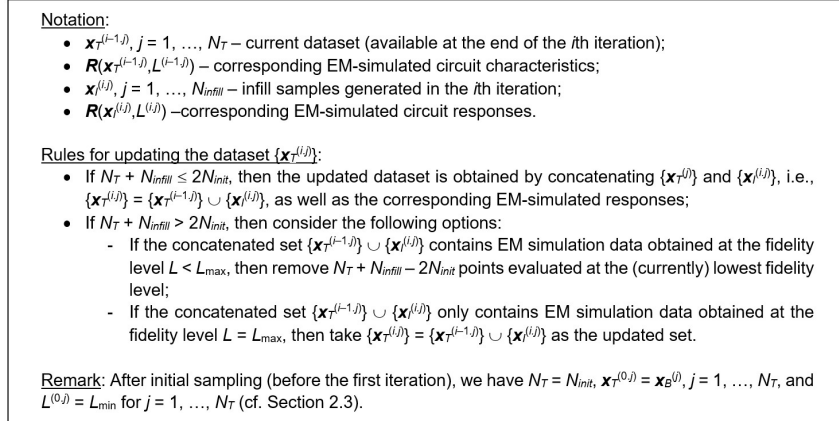


Fig. 4. The employed strategy for dataset updating.

$$F_j = F_{2,\min} + (F_{2,\max} - F_{2,\min})(j - 1)/(N_{infill} - 1) \quad (1)$$

In (1), $F_{2,\min}$ and $F_{2,\max}$ bound the span of the Pareto set (with supplementary conditions). The choice of the infill vectors $\mathbf{x}^{(i,j)}$, $j = 1, \dots, N_{infill}$, has to ensure that they are in close proximity of the assumed levels (here, i refers to the MO procedure iteration index).

A noticeable disparity is observed among the objectives at the surrogate-predicted infill vectors and the respective values assessed based on EM simulation data (which are usually worse due to low accuracy of the ANN). Still, EM-simulated objectives are of prime importance (the surrogate serves merely as a supplementary tool). The quality of the Pareto and the termination condition are evaluated using EM data.

2.6 Management Scheme of Multi-Fidelity Models. Dataset Updating

In order to lower computational expenses, the developed MO framework employs multi-fidelity EM models. In this study, the model fidelity L comes from the range between L_{\min} to L_{\max} . The initial sampling (outlined in Section 2.3) is carried out using L_{\min} . Later, the model resolution is increased until highest fidelity L_{\max} is reached. The latter is crucial for the Pareto-optimal designs to be dependable.

The strategy for managing model fidelity is straightforward and involves an affine adjustment of L . Specifically, in the i th iteration, the resolution $L^{(i)}$ is established as

$$L^{(i)} = \min \left\{ L_{\max}, L_{\min} + (L_{\max} - L_{\min}) \frac{i-1}{N_{\text{transition}}} \right\} \quad (2)$$

where $N_{\text{transition}}$ represents the iteration count beyond which L assumes L_{\max} .

The update of the dataset constitutes a crucial element of the MO procedure because of the involvement of multi-resolution EM models. When only single-resolution model is utilized, addition of the new EM data is simple, i.e., in the i th iteration, we have the complete dataset

$$\{\mathbf{x}_B^{(j)}\}_{j=1,\dots,N_{\text{init}}} \cup \{\mathbf{x}_I^{(1,j)}\}_{j=1,\dots,N_{\text{infill}}} \cup \dots \cup \{\mathbf{x}_I^{(i,j)}\}_{j=1,\dots,N_{\text{infill}}} \quad (3)$$

Whereas in the variable-fidelity approach, the samples of reduced fidelity are systematically eliminated, to ensure that high-fidelity points ultimately persist. Figure 4 illustrates the procedure for dataset updating. The said strategy keeps the dataset of the size up to $2N_{\text{infill}}$ until any samples simulated using $L < L_{\max}$ exist. Later on, the lowest-fidelity points are step-by-step ousted from $\{\mathbf{x}_I^{(i,j)}\}$, until it contains solely high-fidelity. Subsequently, each new ML-rendered sample is directly appended to the set.

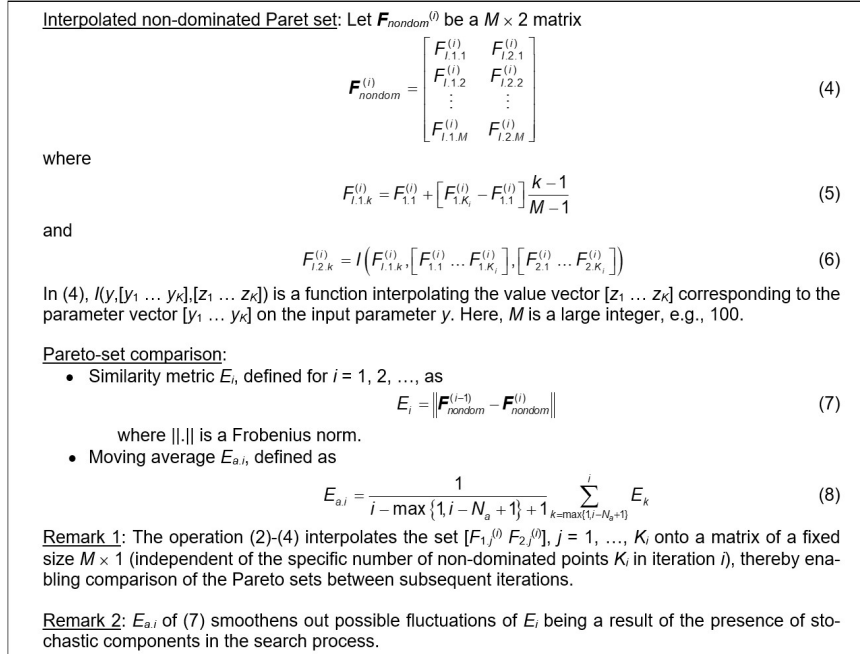


Fig. 5. Termination condition of the introduced ML-based MO procedure.

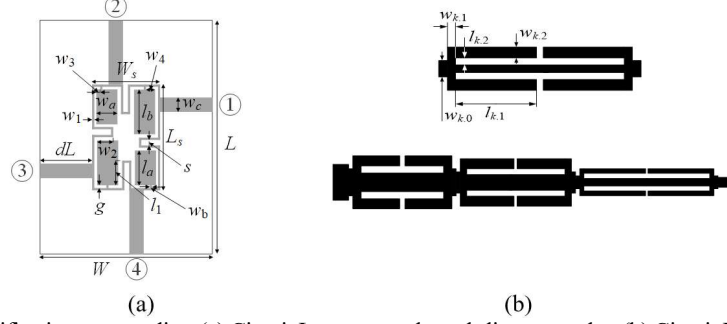


Fig. 6. Verification case studies: (a) Circuit I: a compact branch-linear coupler, (b) Circuit II: a miniaturized three-section 50-to-100 ohm impedance matching transformer; top and bottom panels show the CMRC cell and the entire circuit, respectively.

Table 1. ML-based MO algorithm: Control parameters

Parameter	Description	Default value
N_{init}	Number of initial sample points for building the first ANN surrogate	100
N_{infill}	Number of infill points generated per MO iteration	10
$N_{transition}$	Number of iterations over which the model fidelity is changed from L_{min} to L_{max}	5
N_a	The span of the moving average for Pareto front similarity metric $E_{a,i}$	5
ε	Termination threshold for the MO process	1

2.7 Algorithm Termination

We employ the termination condition based on the similarity of EM-simulated design objectives among the non-dominated designs rendered by successive procedure iterations. The objective vectors are indicated by $[F_{1,j}^{(i)} F_{2,j}^{(i)}], j = 1, \dots, K_i$, and are presumed to be arranged as: $F_{1,j}^{(i)} \leq F_{1,k}^{(i)}$ for $j < k$. The relevant notation is shown in Fig. 5. The termination condition is formulated as $E_{a,1} < \varepsilon$, with ε being the convergence threshold.

2.8 Algorithm Operation

Here, we summarize all the aforementioned algorithmic components. Table 1 gathers the control parameters (five in total) of the proposed ML-base MO procedure. In all numerical experiments, the default values are utilized. In particular, the number N_{init} of initial samples (we use $N_{init} = 100$) can be adjusted in order to achieve the required accuracy of the initial surrogate (e.g., around ten percent of relative RMS error). The remaining parameters are of lesser importance. For example, lower values of N_{infill} permit reducing the cost of each algorithm iteration at the expense of increasing total number of iterations necessary to yield similar Pareto set. Furthermore, higher values of N_a lead to smoothening of the moving average, which might be compensated by increasing ε .

The expenditures associated with the multi-objective (MO) process are evaluated as the total number of EM simulations performed throughout optimization run. Again, MOEA utilizes a fast ANN model, so the overhead of the Pareto set generation are negligible in comparison to the expenses associated with EM circuit simulations. The primary sampling is carried out at the minimum resolution L_{min} . Later on, L is increased to L_{max} (across the

first $N_{transition}$ iterations). As procedure advances, the reduced-fidelity samples are progressively eliminated from the dataset. The gradual enhancement of the distribution of infill vectors within the sub-set comprising the Pareto front leads to the improvement of ANN's accuracy in the very region. The ultimate outcome of our procedure is the high-fidelity Pareto set.

3 Verification Case Studies

Two miniaturized microstrip circuits are utilized to verify the developed MO framework: a branch-line coupler (Circuit I) and a three-section impedance matching transformer (Circuit II), which are shown in Fig. 6. Both circuits employ compact microstrip resonant cells (CMRCs). Table 2 presents all the important details on the verification structures: geometry parameters, substrate, simulation setups, and design goals. All models are simulated using transient solver of CST Microwave Studio.

For both circuits, the parameter spaces are bounded by lower and upper limits on geometry parameters (denoted as \mathbf{l} and \mathbf{u} , respectively). The primary design goal is the same for both structures: minimization of the footprint area. Whereas the secondary goals are as follows: maximization of the 0.5-dB power division band-width (Circuit I), and minimization of the maximal value of reflection level within the assumed band (Circuit II). It is crucial to emphasize that the challenges posed by both test problems primarily arise from high dimensionality of their parameter spaces.

Table 2. Important parameters of verification circuit structures

Circuit	I [46]			II [47]			
Geometry parameters [§] [mm]	$\mathbf{x} = [g \ l_1r \ l_a \ l_b \ w_1 \ w_{2r} \ w_{3r} \ w_{4r} \ w_a \ w_b]^T$			$\mathbf{x} = [l_{1,1} \ l_{1,2} \ w_{1,1} \ w_{1,2} \ w_{1,0} \ l_{2,1} \ l_{2,2} \ w_{2,1} \ w_{2,2} \ w_{2,0} \ l_{3,1} \ l_{3,2} \ w_{3,1} \ w_{3,2} \ w_{3,0}]^T$			
Parameter bounds	Lower $\mathbf{l} = [0.4 \ 0.7 \ 6.0 \ 8.0 \ 0.6 \ 0.85 \ 0.7 \ 0.1 \ 3.0 \ 0.5]^T$			Upper $\mathbf{l} = [2.5 \ 0.15 \ 0.75 \ 0.15 \ 0.3 \ 2.5 \ 0.15 \ 0.18 \ 0.24 \ 1.4 \ 3.0 \ 0.15 \ 0.2 \ 0.25 \ 0.55]^T$			
	Upper $\mathbf{u} = [0.6 \ 0.9 \ 7.0 \ 10 \ 0.9 \ 0.99 \ 0.85 \ 0.3 \ 4 \ 0.7]^T$			Upper $\mathbf{u} = [3.7 \ 0.3 \ 0.8 \ 0.55 \ 0.4 \ 4.5 \ 0.3 \ 0.52 \ 0.55 \ 1.8 \ 4.5 \ 0.5 \ 0.3 \ 0.3 \ 1.5]^T$			
Other parameters [mm]	$L = 2dL + L_s, L_s = 4w_1 + 4g + s + l_a + l_b, W = 2dL + W_s, W_s = 4w_1 + 4g + s + 2w_a, l_1 = lb/l_1r, w_2 = w_a w_{2r}, w_3 = w_3r w_a, \text{ and } w_4 = w_{4r} w_a$			-			
Substrate	RO4003: $\epsilon_r = 3.38, h = 0.51$ mm			RF-35: $\epsilon_r = 3.5, h = 0.762$ mm			
Lowest-fidelity model	LPW (L_{min})	Number of mesh cells	Simulation time [s]	LPW (L_{min})	Number of mesh cells	Simulation time [s]	
	11	~22,000	100	9	~40,000	40	
Highest-fidelity model	LPW (L_{max})	Number of mesh cells	Simulation time [s]	LPW (L_{max})	Number of mesh cells	Simulation time [s]	
	23	~115,000	195	23	~240,000	140	
	F_1	Minimize footprint area [mm ²]: $F_1(\mathbf{x}) = A(\mathbf{x}) = W_s L_s$					
Design goals [‡]		Center frequency: $f_0 = 1.5$ GHz Maximize the power split bandwidth, defined at the (continuous w.r.t. f_0) frequency range for which			Minimize maximum reflection within the band from 1.75 GHz to 4.25 GHz: $F_2(\mathbf{x}) = \max\{f \in [1.75 \ 4.25] \text{ GHz} : S_{11}(\mathbf{x}, f) \}$ Considered are designs for which: $F_2(\mathbf{x}) \leq -$		
		$d_5(\mathbf{x}, f) = S_{21}(\mathbf{x}, f) - S_{31}(\mathbf{x}, f) \leq 0.5$ dB			20 dB		

[§]Parameters with subscript r are relative and unitless.

[‡]Explanation of symbols: $|S_{k1}(\mathbf{x}, f)|$ - scattering parameter S_{k1} , $k = 1, 2, 3, 4$, at design \mathbf{x} and frequency f .

Circuits I and II were optimized using the algorithm developed in the study, as well as the control parameters and their default values (see Table 1). The ultimate result in the form of the Pareto set has been generated, where the non-dominated designs are simulated at the highest admissible fidelity. The benchmark algorithm set is comprehensive, as it comprises three surrogate-assisted MO procedures (summarized in Fig. 7). The two procedures (Algorithm 1 and 2) adhere to a one-shot principle, where a surrogate model is built upfront and subsequently optimized via MOEA so as to establish the Pareto set. The key distinction between the two approaches consists in the choice of metamodel: kriging interpolant (Algorithm 1), and ANN (Algorithm 2). The data sets of two cardinalities are utilized: 400 and 1600 training data samples. Algorithm 3 constitutes a one-fidelity variation of the introduced framework operating solely at the highest model resolution. By comparing our approach with Algorithm 3 we are able to assess the possible computational benefits of integrating multi-fidelity EM simulations into the search process.

Table 3 presents juxtaposition of the computational expenses of the developed algorithm and benchmark techniques, assessed as the equivalent number of highest-fidelity EM simulations of the microwave structure under design. In the case of benchmark algorithms, which use solely high-fidelity EM model, the cost is calculated as the overall number of EM simulations. Figure 8 presents Pareto fronts generated using our methodology and Algorithms 1 through 3. The circuit characteristics pertinent to the designs optimal in the Pareto sense rendered by our algorithm are displayed in Figs. 9 and 10, which have been simulated using fine EM model.

Designs 1 and 3 of Circuit I (presented in Fig. 8) have been fabricated and measured. Figure 11 presents the circuit prototypes, as well as a comparison between the measured and EM-evaluated S-parameters, demonstrating their satisfactory alignment.

The developed multi-fidelity ML-based MO framework outperforms the benchmark algorithms with regard to cost-efficacy and reliability. One-shot methods (Algorithms 1 and 2) produce lesser-quality Pareto fronts as a result of the reduced accuracy of the model built in an unconstrained design space. As far as the reliability of our approach is concerned, it is superior to Algorithms 1 and 2, and similar only to the Algorithm 3. Moreover, employment of multi-fidelity EM simulations does not negatively impact the Pareto set quality.

Table 2. Benchmark algorithms

Algo- rithm	General information	Surrogate model	Characterization
1	One-shot surrogate- assisted MO procedure	Kriging interpolation (Gaussian correlation functions and first-order polynomial) NN (multi-layer perceptron, two hidden layers with ten neurons each; training: Levenberg- Marquardt algorithm)	<ul style="list-style-type: none"> • Surrogate built using N_S data samples, then optimized using MOEA; • Selected non-dominated samples are EM-simulated to yield the final result of the algorithm.
3	Machine learning algorithm with ANN surrogates	ANN surrogates	<ul style="list-style-type: none"> • Initial sampling and surrogate model setup discussed in Section 2.3; • Infill point generation outlined in Section 2.4 and 2.5 (surrogate optimization using MOEA); • EM-evaluated dataset updated by adding all infill points to the existing dataset; • Solely high-fidelity EM model.

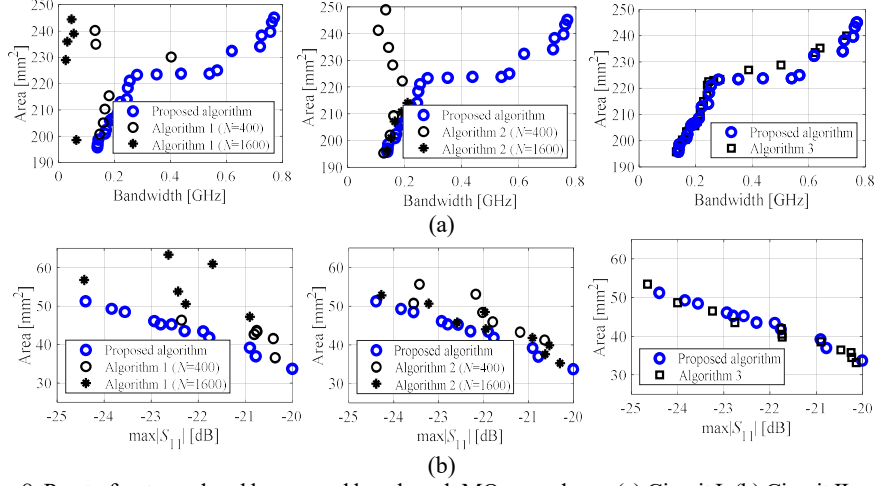


Fig. 8. Pareto fronts rendered by our and benchmark MO procedures: (a) Circuit I, (b) Circuit II.

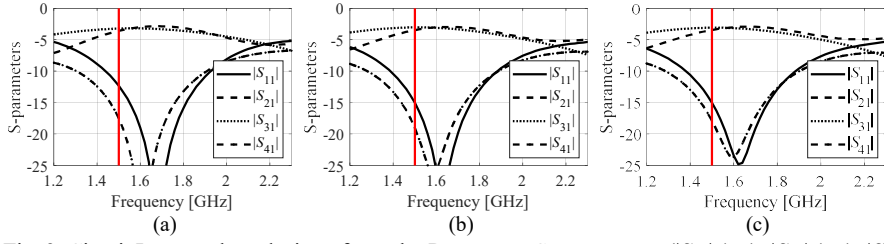


Fig. 9. Circuit I: exemplary designs from the Pareto set, S-parameters ($|S_{11}|$ (—), $|S_{21}|$ (···), $|S_{31}|$ (- - -), $|S_{41}|$ (-o-)) for: (a) $BW = 770$ MHz, $A = 245$ mm² (Design 1), (b) $BW = 620$ MHz, $A = 232$ mm² (Design 2), (c) $BW = 255$ MHz, $A = 221$ mm² (Design 3); $BW - 0.5$ -dB power division bandwidth, $A -$ circuit size. Vertical line shows the intended operating frequency.

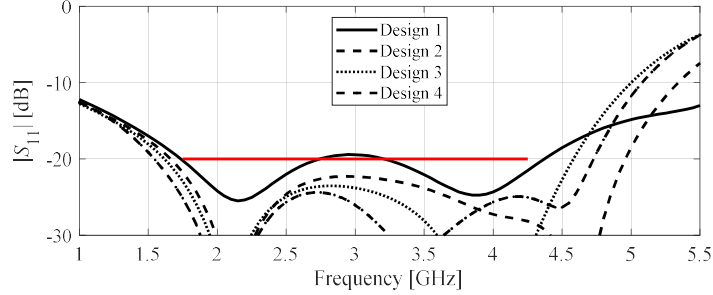


Fig. 10. Circuit II: exemplary designs from the Pareto set, reflection characteristics for: (a) $A = 33.4$ mm² (Design 1), (b) $A = 41.8$ mm² (Design 2), (c) $A = 46.1$ mm² (Design 3), (d) $A = 51.2$ mm² (Design 4). Intended operating frequency range shown by the horizontal line.

The computational efficiency of our framework is considerably better than that of both single-run and ML-based routines: the expenses of our procedure are around 260 high-fidelity EM analyses, whereas for Algorithm 3 it is close to 450 EM analyses (i.e., the savings of 42 percent w.r.t. single-fidelity framework have been obtained without degrading design quality). The relative savings over Algorithms 1 and 2 (using 1600 samples) are even higher (they reach up to 84 percent).

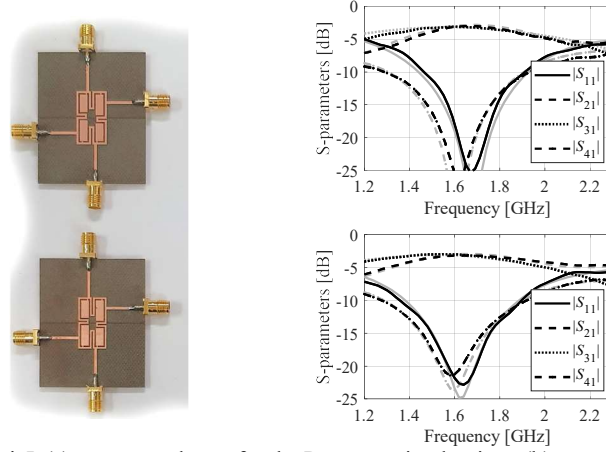


Fig. 11. Circuit I: (a) prototype photos for the Pareto-optimal points; (b) measurements (black) and EM-evaluated (gray) S-parameters. Top and bottom: Designs 1 and 3 of Fig. 8, respectively.

Table 3. Cost breakdown: the developed and benchmark procedures

Algorithm	Optimization cost [#]	
	Circuit I	Circuit II
This work	306.6	212.3
1	$N = 400$	400
	$N = 1600$	1600
2	$N = 400$	400
	$N = 1600$	1600
3	500	390

[#] The cost of benchmark algorithms is assessed as the overall count of executed EM simulations. In the proposed approach, the cost is appraised as the equivalent number of high-fidelity EM simulations, considering the time evaluation ratio between the high- and lower-fidelity models.

4 Conclusion

This work proposed an innovative approach for accelerated multi-objective optimization of compact microwave devices. Our methodology revolves around a machine learning framework utilizing an artificial neural network (ANN) model. At each iteration of the search procedure, multiple infill points are generated and integrated into the dataset, progressively refining the surrogate model. Intermediate representations of the Pareto front are crafted by optimization of the ANN surrogate using a multi-objective evolutionary algorithm, driving designs toward the Pareto front. Additionally, the incorporation of variable-resolution EM simulations, managed by a tailored model management strategy, further enhances cost-efficiency. Rigorous numerical validation showcases the exceptional computational efficiency of our method (averaging fewer than three hundred high-fidelity EM simulations per optimization run) and its reliability compared to various surrogate-assisted and machine learning benchmark algorithms.

Acknowledgement

The authors would like to thank Dassault Systemes, France, for making CST Microwave Studio available. This work is partially supported by the Icelandic Centre for Research (RANNIS) Grant 239858 and by National Science Centre of Poland Grant 2022/47/B/ST7/00072.

References

1. Al Khanjar, K., Djerafi, T.: Highly reconfigurable patch coupler with frequency and power-dividing ratio control for millimeter-wave applications. *IEEE Trans. Microwave Theory Techn.*, **71**, pp. 2118–2128 (2023)
2. Li, Q., Chen, X., Ch, P., Yang T.: Tunable bandstop filter using distributed coupling microstrip resonators with capacitive terminal. *IEEE Microwave Wireless Comp. Lett.*, **30**, pp. 35–38 (2020)
3. Tian, H., Dong, Y.: Wideband low-loss filter with compact size and wide stopband based on folded planar waveguide. *IEEE Microwave Wireless Techn. Lett.*, **33**, pp. 651–654 (2023)
4. Arsanjani, A., Bartlett, C., Robins, L., Teschl, R., Bösch, W., Höft M.: Metasurfaces for filter miniaturization and out-of-band rejection improvement. *IEEE Microwave Wireless Techn. Lett.*, **33**, pp. 271–274 (2023)
5. Zhu, F., Wu, Y., Zhao, X., Chu, P., Luo, G.Q., Wu K.: Compact and wide stopband bandpass filters based on dual-mode folded circular substrate integrated waveguide cavities. *IEEE Trans. Microwave Theory Techn.*, **71**, pp. 3102–3113 (2023)
6. Hussain, N., Kim, N.: Integrated microwave and mm-wave MIMO antenna module with 360° pattern diversity for 5G Internet of Things. *IEEE Internet of Things J.*, **9**, pp. 24777–24789, 2022
7. Ilyas, S., Shoaib, N., Nikolaou, S., Cheema H.M.: A wideband tunable power divider for SWIPT systems. *IEEE Access*, **8**, pp. 30675–30681 (2020)
8. Yang, L., Zhou, Y.J., Zhang, C., Yang, X.M., Yang, X., Tan C.: Compact multiband wireless energy harvesting based battery-free body area networks sensor for mobile healthcare. *IEEE J Electromagn RF Microw Medicine Biology*. **2**, pp. 109–115 (2028)
9. Letavin, D.: Miniature microstrip branch line coupler with folded artificial transmission lines. *Int J Electron Commun.*, **99**, pp. 8–13 (2019)
10. Qian, Z.Y., Chen, J.X.: Compact bandpass filter using CMRC-based dual-behavior resonator. *Int. J. RF Microwave CAE*, **29**, e21719 (2019)
11. Chen, S., Guo, M., Xu, K., Zhao, P., Dong, L., Wang G.: A frequency synthesizer based microwave permittivity sensor using CMRC structure. *IEEE Access*, **6**, pp. 8556–8563 (2018)
12. Zhu, D.Z., Werner, P.L., Werner D.H.: Design and optimization of 3-D frequency-selective surfaces based on a multiobjective lazy ant colony optimization algorithm. *IEEE Trans. Ant. Propag.*, **65**, pp. 7137–7149 (2017)
13. Bandler, J.W., Rayas-Sánchez, J.E.: An early history of optimization technology for automated design of microwave circuits. *IEEE J. Microwaves*, **3**, pp. 319–337 (2023)
14. Zhang, W., Feng, F., Gongal-Reddy, V.W.R., Zhang, J., Yan, S., Zhang Q.J.: Space mapping approach to electromagnetic centric multiphysics parametric modeling of microwave components. *IEEE Trans. Microwave Theory Techn.*, **66**, pp. 3169–3185 (2018)

15. Zhang, W., Feng, F., Liu, W., Yan, S., Zhang, J., Jin, J., Zhang, Q.J.: Advanced parallel space-mapping-based multiphysics optimization for high-power microwave filters. *IEEE Trans. Microwave Theory Techn.*, **69**, pp. 24702484 (2021)
16. Zhang, Z., Cheng, Q.S., Chen, H., Jiang F.: An efficient hybrid sampling method for neural network-based microwave component modeling and optimization. *IEEE Microwave Wireless Comp. Lett.*, **30**, pp. 625–628 (2020)
17. Pietrenko-Dabrowska, A., Koziel, S.: *Response feature technology for high-frequency electronics. Optimization, modeling, and design automation*, Springer, New York, 2023.
18. Wu, Q., Wang, H., Hong W.: Multistage collaborative machine learning and its application to antenna modeling and optimization. *IEEE Trans. Ant. Propag.*, **68**, pp. 3397–3409 (2020)
19. Koziel, S., Pietrenko-Dabrowska, A.: Efficient gradient-based algorithm with numerical derivatives for expedited optimization of multi-parameter miniaturized impedance matching transformers. *Radioengineering*, **28**, pp. 572–578 (2019)
20. Deb, K.: *Multi-Objective Optimization Using Evolutionary Algorithms*. Wiley, New York, 2001.
21. Marler, R.T., Arora, J.S.: The weighted sum method for multi-objective optimization: new insights. *Structural Multidisc. Opt.*, **41**, pp. 853–862 (2010)
22. Ghorbaninejad, H., Heydarian, R.: New design of waveguide directional coupler using genetic algorithm. *IEEE Microwave Wireless Comp. Lett.*, **26**, pp. 86–88 (2016)
23. Baumgartner, P., Baurnefeind, T., Biro, O., Hackl, A., Magele, C., Renhart, W., Torchio R.: Multi-objective optimization of Yagi-Uda antenna applying enhanced firefly algorithm with adaptive cost function. *IEEE Trans. Magnetics*, **54**, article no. 8000504 (2018)
24. Liu, C., Zheng, F., Kai C.: An improved multi-objective artificial bee colony algorithm for pattern synthesis of conformal arrays. *Int. Conf. Natural Computation. Int. Conf. Natural Computation, Fuzzy Systems and Knowledge Discovery (ICNC-FSKD)*, Changsha, pp. 265–270 (2016)
25. Champasak, P., Panagant, N., Pholdee, N., Bureerat, S., Yildiz, A.R.: Self-adaptive many-objective meta-heuristic based on decomposition for many-objective conceptual design of a fixed wing unmanned aerial vehicle, *Aerospace Science Techn.*, **100**, art. no. 105783 (2020)
26. Al-Tashi, Q., Abdulkadir, S.J., Rais, H.M., Mirjalili, S., Alhussian H.: Approaches to multi-objective feature selection: A systematic literature review. *IEEE Access*, **8**, pp. 125076–125096 (2020)
27. Yang, W., Li, Y., Wang, H., Jiang, M., Cao, M., Liu „Multi-objective optimization of high-power microwave sources based on multi-criteria decision-making C. *IEEE Trans. Electron Dev.*, **70**, pp. 3892–3898 (2023)
28. Wei, Y., Qi, G., Wang, Y., Yan, N., Zhang, Y., Feng L.: Efficient microwave filter design by a surrogate-model-assisted decomposition-based multi-objective evolutionary algorithm. *Electronics*, **11**, pp. 3309 (2022)
29. De Melo, M.C., Santos, P.B., Faustino, E., Bastos-Filho, C.J.A., Sodr e A.C.: Computational intelligence-based methodology for antenna development. *IEEE Trans. Ant. Propag.*, **10**, pp. 1860–1870 (2022)
30. Wu, W., Wang, H., Hong W.: Multistage collaborative machine learning and its application to antenna modelling and optimization. *IEEE Trans. Ant. Propag.*, **68**, pp. 3397–3409 (2020)
31. Nouri, M., Aghdam, S.A., Jafarieh, A., Mallat, N.K., Jamaluddin, M.H., Dor-Emami M.: An optimized small compact rectangular antenna with meta-material based on fast multi-objective optimization for 5G mobile communication. *J. Comp. Electr.*, **20**, pp. 1532–1540 (2021)

32. Liu, B., Aliakbarian, H., Radiom, S., Vandenbosch, G.A.E., Gielen G.: Efficient multi-objective synthesis for microwave components based on computational intelligence techniques. in *Des. Automat. Conf. (DAC)*. San Francisco, CA, pp. 542–548 (2012)
33. An, S., Yang, S., Mohammed O.A.: A Kriging-assisted light beam search method for multi-objective electromagnetic inverse problems. in *IEEE Trans. Magn.*, **54**, paper 7001104, (2018)
34. Taran, N., Ionel, D.M., Dorrell D.G.: Two-level surrogate-assisted differential evolution multi-objective optimization of electric machines using 3-D FEA. *IEEE Trans. Magn.*, **54**, paper 8107605 (2018)
35. Koziel, S., Pietrenko-Dabrowska, A.: Constrained multi-objective optimization of compact microwave circuits by design triangulation and Pareto front interpolation. *European J. Op. Research.*, **299**, pp. 302–312 (2022)
36. Koziel, S., Pietrenko-Dabrowska, A., Performance-driven surrogate modeling of high-frequency structures, Springer, New York, 2020.
37. Pietrenko-Dabrowska, A., Koziel, S., Golunski L.: Two-stage variable-fidelity modeling of antennas with domain confinement. *Sc. Rep.*, **12**, paper No. 17275 (2022)
38. Pietrenko-Dabrowska, A., Koziel, S.: Accelerated multi-objective design of miniaturized microwave components by means of nested kriging surrogates. *Int. J. RF & Microwave CAE.*, **30**(4), paper No. e22124 (2020)
39. Koziel, S., Pietrenko-Dabrowska, A.: Fast multi-objective optimization of antenna structures by means of data-driven surrogates and dimensionality reduction. *IEEE Access.*, **8**, pp. 183300–183311 (2020)
40. Deb, K. *Multi-objective optimization using evolutionary algorithms*. Wiley, New York, 2001.
41. Koziel, S., Pietrenko-Dabrowska, A., Accelerated gradient-based optimization of antenna structures using multi-fidelity simulation models. *IEEE Trans. Ant. Propag.*, **69**(12), pp. 8778-8789 (2021).
42. Beachkofski, B., Grandhi, R. Improved distributed hypercube sampling. American Institute of Aeronautics and Astronautics, paper AIAA 2002–1274 (2002).
43. Vang-Mata, R. (Ed.) *Multilayer perceptrons*, Nova Science, Hauppauge, NY, 2020.
44. Fonseca, C.M., Fleming, P.J. Multiobjective optimization and multiple constraint handling with evolutionary algorithms—Part I: a unified formulation. *IEEE Trans. Syst. Man Cybernetics: Part A: Syst. Humans*, **28**(1), pp. 26–37 (1998).
45. Michalewicz, Z. *Genetic algorithms + data structures = evolution programs*, Springer, New York, 1996.
46. Tseng, C.H., Chang, C.L. A rigorous design methodology for compact planar branch-line and rat-race couplers with asymmetrical T-structures. *IEEE Trans. Microwave Theory Techn.*, **60**(7), pp. 2085–2092 (2012).
47. Koziel, S., Pietrenko-Dabrowska, A., Reliable data-driven modeling of high-frequency structures by means of nested kriging with enhanced design of experiments. *Eng. Comp.*, **36**(7), pp. 2293–2308 (2019).